E7-2026-41

I. I. Ulanova[1,*], A. V. Isaev[1], R. S. Mukhin[1], I. N. Izosimov[1], G. Kaminski[1], A. V. Karpov[1], O. N. Malyshev[1], Yu. A. Popov[1], E. A. Sokol[1], A. M. Solntsev[1], V. I. Chepigin[1], A. I. Svirikhin[1]

A TIME-PROJECTION CHAMBER FOR STUDIES OF SPONTANEOUS FISSION OF SUPERHEAVY NUCLEI

Submitted to "Natural Science Review"

[1] Joint Institute for Nuclear Research, Dubna, Russia
[*] E-mail: ulanova@jinr.ru

Уланова И. И. и др. E7-2026-41

Время-проекционная камера для исследований спонтанного деления сверхтяжелых ядер

Представлена концепция время-проекционной камеры для исследований спонтанного деления сверхтяжелых ядер, доставляемых в фокальную плоскость сепаратора ядер отдачи. Детектор предназначен для ядер, образующихся в ядерных реакциях, сепарируемых от первичного пучка и останавливаемых в газе после входного окна, что позволяет совместить сепарацию ядер отдачи с трехмерной реконструкцией треков осколков деления.

Концепция направлена на получение информации о кинематике осколков, включая полную кинетическую энергию, массы и редкие моды деления; совместимость с SFiNx может обеспечить корреляции с мгновенными нейтронами.

Моделирование Geant4 использовано для оптимизации геометрии камеры, толщины входного окна и давления газа в условиях фокальной плоскости GRAND; определена область, где окно остается механически устойчивым, а детектор сохраняет чувствительность к событиям спонтанного деления. Результаты показывают, что такая камера может расширить возможности исследований спонтанного деления ядер.

Работа выполнена в Лаборатории ядерных реакций им. Г. Н. Флерова ОИЯИ.

Препринт Объединенного института ядерных исследований. Дубна, 2026

Ulanova I. I. et al. E7-2026-41

A Time-Projection Chamber for Studies of Spontaneous Fission of Superheavy Nuclei

A concept of a time-projection chamber for studies of spontaneous fission of superheavy nuclei delivered to the focal plane of a recoil separator is presented. The detector is intended for nuclei produced in nuclear reactions separated from the primary beam and stopped in the gas after the entrance window, making it possible to combine recoil separation with three-dimensional reconstruction of fission-fragment tracks.

The concept is aimed at obtaining information on fragment kinematics, including total kinetic energy, masses, and rare fission modes; compatibility with SFiNx would allow correlations with prompt neutrons.

Geant4 simulations were used to optimize the chamber geometry, entrance-window thickness, and gas pressure for the GRAND focal-plane conditions; an operating region was determined where the window remains mechanically safe and the detector preserves sensitivity to spontaneous-fission events. The results show that such a chamber can extend experimental capabilities for studying spontaneous fission of nuclei.

The investigation has been performed at the Flerov Laboratory of Nuclear Reactions, JINR.

Preprint of the Joint Institute for Nuclear Research. Dubna, 2026

INTRODUCTION

Spontaneous fission of heavy and superheavy nuclei is one of the most sensitive probes of nuclear structure at the limits of stability. The process is governed by the interplay between Coulomb repulsion, shell effects, collective deformation, and the redistribution of excitation energy between the nascent fragments. Fragment mass distributions, total kinetic energy (TKE), and prompt-neutron emission are therefore essential observables for characterizing the mass-energy division in fission and the excitation energy carried by the fragments after scission.

For transfermium and superheavy nuclei, experimental data remain scarce because production cross sections are small, lifetimes are often short, and the number of registered decay events is limited. Under such conditions, each spontaneous-fission event should provide as much information as possible.

At the Flerov Laboratory of Nuclear Reactions (FLNR, JINR), short-lived heavy nuclei are produced in heavy-ion reactions and transported to the focal-plane detector system after separation from the primary beam and background reaction products. In the present experimental approach, the separated nuclei are implanted into a silicon-detector assembly, where subsequent α decays and spontaneous-fission events are registered. The SFiNx neutron detector [1, 2] surrounding the focal-plane detection system makes it possible to measure prompt neutrons from spontaneous fission.

Silicon detector systems are highly efficient for decay-chain identification and for the registration of spontaneous-fission events. In particular, double-sided silicon detectors provide position and energy information for implanted nuclei, α particles, and fission fragments. However, this technique provides only limited event-by-event information on fission-fragment kinematics. The measured fragment energies can be affected by dead layers, detector thresholds, entrance foils, pulse-height defects, and geometrical losses, while the fragment ranges in the detector material are not reconstructed directly. As a result, the determination of TKE and fragment masses remains limited.

A time-projection chamber (TPC) offers a different experimental approach. In a gas-filled active volume, charged fission fragments produce ionization tracks, which can be used to reconstruct their ranges and energy-loss profiles. After appropriate calibration, this information can provide event-by-event access to fission-fragment kinematics, including TKE and fragment masses.

Conventional fission TPCs are usually designed for measurements with a fissioning source placed inside the active volume. This geometry is not

directly applicable to experiments with superheavy nuclei produced in nuclear reactions and transported to the focal plane of a separator system. The present work therefore proposes a TPC concept adapted for separator-delivered superheavy nuclei. In the proposed configuration, the fissioning nucleus is produced in a nuclear reaction, separated by the GRAND gas-filled recoil analyzer, and stopped in the active gas volume of the chamber.

The aim of the present work is to develop and simulate a separator-coupled TPC for studies of spontaneous fission of superheavy nuclei. The paper describes the detector concept, the Geant4-based simulation model, the optimization of gas pressure and entrance-window thickness, and the evaluation of the expected registration efficiency under conditions relevant to experiments at the GRAND focal plane.

1. EXPERIMENTAL MOTIVATION AND EXISTING DETECTOR CONFIGURATION

1.1. GRAND as a basis for the proposed TPC configuration. The proposed TPC is considered as a possible focal-plane detection system for GRAND, the Gas-filled Recoil Analyzer and Nuclei Detector of the Superheavy Element Factory at FLNR. The GRAND separator is designed for experiments with nuclei produced in heavy-ion reactions and operates in a gas-filled mode, with helium or hydrogen considered as working gases [3, 4].

The GRAND focal plane can accommodate different detector systems depending on the experimental task, including chemical chambers, spectrometric detection systems, setups for nuclear mass measurements, and dedicated detectors for fission studies (Fig. 1). In this context, the proposed TPC represents a specialized focal-plane detector for fission studies.



Fig. 1. General view of GRAND at the Superheavy Element Factory of FLNR

A simplified schematic layout of the GRAND separator and its focal-plane region is shown in Fig. 2.

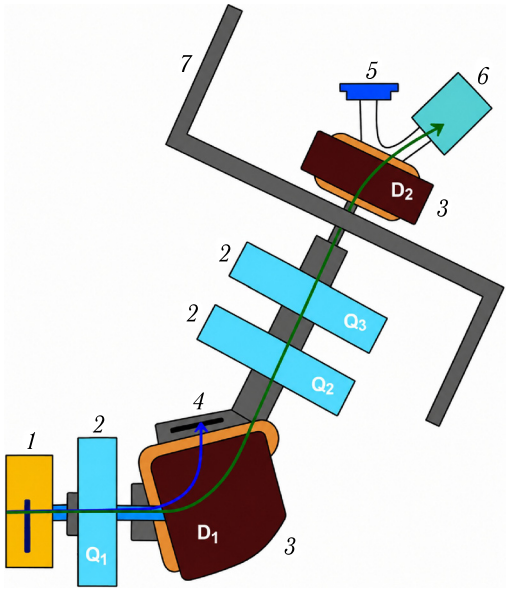


Fig. 2. Simplified schematic layout of the GRAND separator. *1* — target chamber; *2* — quadrupole lenses; *3* — dipole magnets; *4* — beam stopper, into which the primary beam is directed; *5* — detector system for chemical experiments; *6* — detector system for physical experiments; *7* — shielding wall for reducing the radiation background in the focal plane

1.2. Limitations of silicon-detector measurements of fission fragments. Despite its high efficiency for decay-chain identification, the approach based on silicon detectors has limitations for precise measurements of fission-fragment energies. Silicon detectors register the energy deposited by a fragment in an individual detector element, but the measured signal does not always correspond to the full fragment kinetic energy.

The main limitation is related to energy losses and pulse-height defects for heavy ions. The measured fragment energies can be affected by dead layers, detector thresholds, entrance foils, incomplete charge collection, pulse-height defects, and geometrical losses. These effects complicate the reconstruction of the TKE of the two fission fragments.

As a result, the extraction of fragment masses on an event-by-event basis remains limited in the existing configuration based on silicon detectors. A gas-filled TPC can address this problem by measuring the fragment tracks and energy-loss profiles in the active volume. After appropriate calibration, such information may provide additional constraints for the reconstruction of TKE and fragment masses.

2. CONCEPT OF THE SEPARATOR-COUPLED TIME-PROJECTION CHAMBER

2.1. General detector concept. The proposed detector concept is based on a TPC placed at the focal plane of GRAND. It is intended for event-by-event studies of spontaneous fission of nuclei produced in heavy-ion reactions, separated by GRAND, and stopped in the active gas volume of the chamber.

In contrast to conventional source-based fission TPC measurements, the fissioning nucleus is not introduced as a stationary source inside the detector. Instead, the separated recoil nucleus enters the chamber through a thin entrance window and loses its residual kinetic energy in the gas. If spontaneous fission occurs after stopping, the emitted fragments produce ionization in the active volume. The ionization electrons drift toward the readout plane, where the charge distribution and drift-time information are recorded.

In this configuration, the active gas volume both stops separator-delivered recoil nuclei and serves as the detection volume for fission fragments. After appropriate calibration, the measured track and energy-loss information may be used to constrain fission-fragment kinematics, including TKE and fragment masses. Therefore, the chamber dimensions, gas pressure, entrance-window thickness, and readout geometry must be optimized together.

2.2. Difference from conventional TPC configurations. Time-projection chambers have been used in fission studies as active gas detectors for measuring charged fission fragments [5]. In conventional fission TPC configurations, the fissioning material is usually placed inside the active volume, either as a spontaneous-fission source or as an actinide target irradiated by an external neutron beam. In this case, fission fragments are emitted directly into the surrounding gas from a fixed source position.

Gas-filled TPCs with other readout schemes have also been used for studies of rare nuclear decays. For example, the Warsaw Optical TPC was applied to decay studies of very neutron-deficient Zn isotopes, where exotic nuclei were stopped in a gas volume and charged-particle tracks from proton emission were recorded using optical readout [6].

In contrast, the TPC proposed in the present work is intended for separator-delivered recoil nuclei. Therefore, it must be optimized simultaneously for recoil transmission, recoil stopping in the active gas volume, and fission-fragment registration.

2.3. Concept of the GRAND-coupled TPC. Figure 3 summarizes the proposed GRAND-coupled TPC concept and shows the main elements of the detector geometry considered in the present work.

2.4. Requirements for operation at the GRAND focal plane. Operation of the proposed TPC at the GRAND focal plane requires a compromise between recoil transmission, recoil stopping, and fission-fragment detection. The entrance window must be thin enough to transmit evaporation residues with minimal energy loss and angular straggling, while remaining

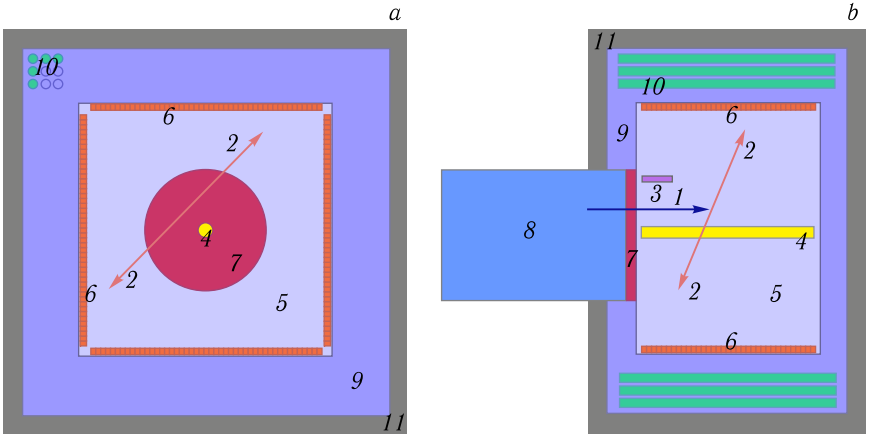


Fig. 3. Concept of the time-projection chamber for spontaneous-fission registration in the separator-coupled configuration: front view (*a*) and side view (*b*). *1* — incoming evaporation residue delivered by GRAND; *2* — fission fragments emitted after spontaneous fission; *3* — position of the calibration source; *4* — cathode; *5* — active gas volume of the time-projection chamber; *6* — anodes; *7* — Mylar separating foil; *8* — ion-guide channel of the GRAND separator; *9* — polyethylene neutron moderator; *10* — ^{3}He neutron counters; *11* — background-neutron shielding made of polyethylene containing 5% boron

mechanically stable under the pressure difference between the detector gas and the beam-line vacuum.

The gas pressure must be chosen so that incoming recoil nuclei stop inside the active volume. At the same time, the pressure should not be so high that the fission-fragment ranges in the gas become too short for reconstruction of track and energy-loss information. Thus, the pressure determines both the stopping efficiency for separator-delivered nuclei and the quality of fission-fragment measurements.

The active volume must be large enough to contain a significant part of the fission-fragment tracks, while remaining compatible with the geometrical constraints of the GRAND focal plane. These requirements define the main parameters to be optimized in the simulation: entrance-window thickness, gas pressure, chamber geometry, and the resulting registration efficiency.

3. MATERIAL AND METHODS

3.1. Detector geometry. The detector geometry used in the present study was implemented in the Geant4 simulation toolkit [7, 8]. The model represents a compact cubic TPC with an outer size of $15.5 \times 15.5 \times 15.5$ cm (Fig. 4). This size corresponds to the central region available inside the SFiNx neutron-detector assembly and defines the maximum geometrical envelope used in the simulation.

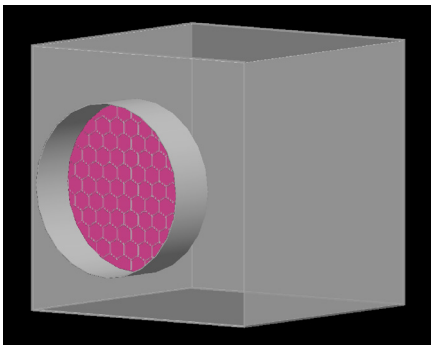


Fig. 4. Three-dimensional Geant4 model of the proposed compact TPC geometry

The chamber housing was modeled as a stainless-steel vessel with a wall thickness of 1 mm. The wall thickness was fixed in the present simulation and was not included among the optimized parameters.

The entrance side of the chamber contains a circular entrance window with a diameter of 10 cm. The window defines the geometrical acceptance for evaporation residues entering the detector from GRAND. In the optimization procedure, the window thickness was varied together with the gas pressure.

The sensitive volume was filled with an argon–butane mixture, Ar + + C_4H_{10}. Argon–isobutane mixtures have been used as drift gases in fission TPC detectors, including the NIFFTE fission TPC [5]. In the present work, this mixture was chosen as the baseline working gas for the simulation of highly ionizing fission fragments. Argon provides the main ionization gas, while butane acts as a quenching component. The mass fractions used in the Geant4 material definition were 93% for argon and 7% for butane.

At atmospheric pressure, the gas density was taken as

$$\rho_{\mathrm{mix}}(1\ \mathrm{atm}) = 0.00170\ \mathrm{g/cm^3}.$$

For other pressures, the density was scaled linearly at a fixed temperature of 293.15 K. This approximation allows the stopping power of the gas volume to be varied through the gas pressure while keeping the gas composition fixed.

The charge readout of the proposed detector is based on a Micromegas structure [9]. In the present model, the Micromegas plane is introduced as the readout boundary of the active volume. It provides the two-dimensional projection of the ionization charge, while the third coordinate is obtained from the electron drift time. Avalanche multiplication, electronics response, and detailed signal formation were not simulated at this stage.

3.2. Recoil-nucleus source and beam distribution. The source of recoil nuclei was modeled using the experimentally determined spatial profile of the beam at the exit of the GRAND separator. This approach was introduced in order to avoid the idealized approximation of a pencil-like beam and to account for the finite transverse size of the recoil distribution at the detector

entrance. The use of an experimentally motivated beam profile is important because the initial position of a recoil nucleus determines whether it enters the active region of the TPC and how the subsequent fission-fragment tracks are distributed inside the detector volume.

The spatial distribution was based on the data obtained at the focal plane of the GRAND separator for nuclei produced in the reaction

$$^{206}\mathrm{Pb}(^{48}\mathrm{Ca}, 2n)^{252}\mathrm{No}. \tag{1}$$

The number of registered recoil nuclei was determined in concentric radial intervals with a step of 6 mm. The experimental data used for the construction of the source distribution are given in Table 1.

Table 1. **Experimental radial distribution of recoil nuclei at the focal plane of the GRAND separator used for the source model**

Radius r_i, mm	Number of particles N_i
6	1700
12	1367
18	1351
24	1419
30	1258
36	1049
42	1004
48	902

Let r_i be the radius corresponding to the i-th radial interval and let N_i be the number of particles registered in this interval. The total number of particles in the experimental profile is

$$N_\Sigma = \sum_{i=1}^{n} N_i, \tag{2}$$

where n is the number of radial intervals. The probability of generating a recoil nucleus in the i-th radial interval was then defined as the normalized experimental frequency

$$P_i = \frac{N_i}{N_\Sigma} = \frac{N_i}{\sum_{j=1}^{n} N_j}. \tag{3}$$

By construction, the probabilities satisfy the normalization condition

$$\sum_{i=1}^{n} P_i = 1. \tag{4}$$

For use in the Monte Carlo event generator, the discrete probability distribution was transformed into a cumulative distribution function. The

cumulative probability up to the k-th radial interval was defined as

$$F_k = \sum_{i=1}^{k} P_i, \qquad F_0 = 0, \qquad F_n = 1. \tag{5}$$

This cumulative distribution was used to sample the radial coordinate by the inverse-transform method. For each simulated event, a random number

$$\xi \sim U(0,1) \tag{6}$$

was generated. The radial interval was selected from the condition

$$F_{k-1} < \xi \leqslant F_k. \tag{7}$$

If condition (7) was fulfilled, the radial coordinate of the recoil nucleus was assigned to the corresponding interval characterized by r_k.

After the radial interval had been selected, the azimuthal angle was generated independently from a uniform distribution,

$$\varphi \sim U(0, 2\pi). \tag{8}$$

The initial transverse coordinates of the recoil nucleus in the entrance plane of the detector were then calculated as

$$x = x_0 + r_k \cos\varphi, \qquad y = y_0 + r_k \sin\varphi, \tag{9}$$

where (x_0, y_0) denotes the center of the beam spot. Thus, the experimentally measured radial distribution was converted into a two-dimensional transverse source distribution.

The corresponding experimental radial profile is shown in Fig. 5. The decrease in N_i with increasing r_i reflects the fact that the density of separator-delivered recoil nuclei is highest near the beam axis and decreases toward the periphery.

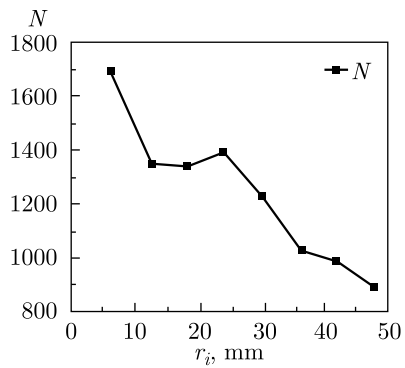


Fig. 5. Experimental radial distribution of recoil nuclei at the focal plane of the GRAND separator used for the source model. The distribution was obtained from the number of registered nuclei in concentric radial intervals

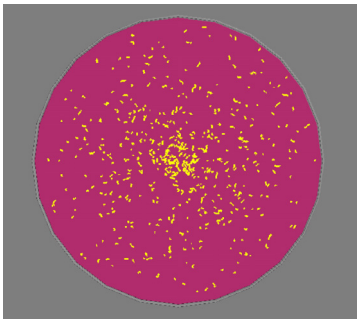


Fig. 6. Geant4 visualization of the modeled recoil-nucleus distribution at the entrance region of the proposed TPC. The finite transverse size of the beam was generated using the experimentally motivated radial distribution

A Geant4 visualization of the generated recoil distribution in the entrance region of the detector is shown in Fig. 6. The simulated trajectories demonstrate that the source model reproduces the finite transverse size of the separator-delivered recoil beam and its overlap with the entrance region of the proposed TPC.

3.3. Energy distribution of recoil nuclei. In addition to the transverse beam profile, the initial kinetic-energy distribution of recoil nuclei was included in the source model. This parameter determines the transmission of evaporation residues through the entrance window and their stopping in the active gas volume.

The energy distribution (Fig. 7) was based on the experimental spectrum measured at GRAND for evaporation residues produced in the reaction

$$^{206}\mathrm{Pb}(^{48}\mathrm{Ca}, 2n)^{252}\mathrm{No}. \tag{10}$$

The experimental spectrum was used as the basis for the recoil-energy generation in the new simulation. The distribution was approximated by a Gaussian function with the mean value

$$E_0 = 17 \text{ MeV} \tag{11}$$

and the standard deviation

$$\sigma_E = 2.5 \text{ MeV}. \tag{12}$$

For each simulated event, the initial kinetic energy of the ^{252}No recoil nucleus was sampled from this distribution,

$$E \sim \mathcal{N}(E_0, \sigma_E). \tag{13}$$

This approach accounts for the experimentally observed energy spread of nuclei delivered by GRAND and avoids the assumption of monoenergetic recoil injection.

The generated distribution reproduces the mean energy and finite width of the experimental recoil spectrum. These parameters were then used in the

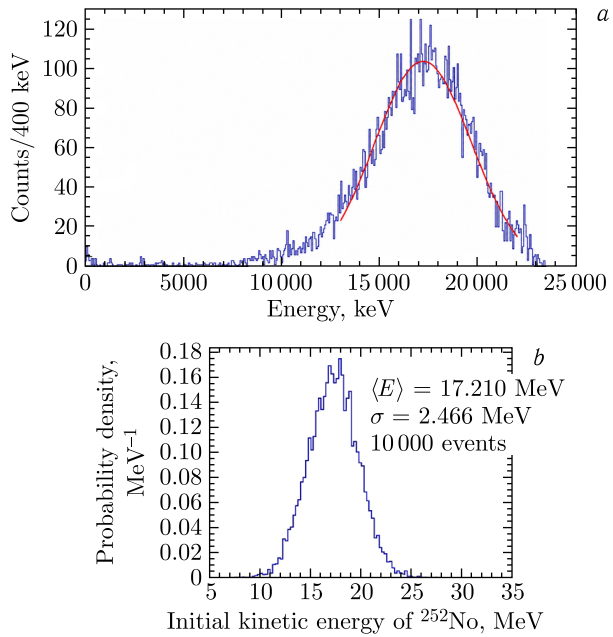


Fig. 7. Energy distributions of ^{252}No recoil nuclei used in the source model. *a*) Experimental kinetic-energy distribution measured at GRAND for evaporation residues produced in the ^{206}Pb(^{48}Ca, $2n$)^{252}No reaction. *b*) Simulated kinetic-energy distribution of primary ^{252}No recoil nuclei sampled from a Gaussian distribution with $E_0 = 17$ MeV and $\sigma_E = 2.5$ MeV

detector-response simulation for the transport of ^{252}No nuclei through the entrance region and their stopping in the active gas volume.

3.4. Spontaneous-fission event generation. The spontaneous-fission event generator was implemented in Geant4 as a user-defined model for the decay of stopped ^{252}No recoil nuclei inside the active detector volume. In the present work, the spontaneous fission of ^{252}No was not described by independently sampled fragment masses and energies. Instead, complete event-by-event fission information was taken from the GEF code [10], which allows one to preserve the physical correlations between fragment masses, fragment charges, TKE, and prompt-neutron emission.

The fission-event library was generated using GEF version 2024/1.1 in the spontaneous-fission mode for the nucleus:

$$Z_0 = 102, \qquad A_0 = 252, \tag{14}$$

with the extended `lmd+` option enabled. In this mode, GEF provides an event-by-event list of spontaneous-fission observables, including the fragment properties after prompt-neutron emission, the total post-neutron kinetic

energy, and the characteristics of emitted prompt neutrons. A total of 10^5 spontaneous-fission events were generated in advance and used as the source library for the Geant4 simulation.

The original GEF output was converted into a compact event file containing, for each spontaneous-fission event, the fragment charges and post-neutron masses,

$$Z_L,\ A_{L,\mathrm{post}},\ Z_H,\ A_{H,\mathrm{post}}, \tag{15}$$

the post-neutron TKE,

$$\mathrm{TKE}_{\mathrm{post}}, \tag{16}$$

and the prompt-neutron multiplicities from the light and heavy fragments,

$$\nu_L,\ \nu_H, \tag{17}$$

together with the energies and angular coordinates of all prompt neutrons belonging to that event. Here the subscript "post" denotes fragment properties after prompt-neutron emission.

The generated GEF event library contains 100 000 spontaneous-fission events. Its mean prompt-neutron multiplicity is

$$\langle \nu \rangle = 4.3, \tag{18}$$

the mean prompt-neutron energy is

$$\langle E_n \rangle = 2.4\ \mathrm{MeV}, \tag{19}$$

and the mean total post-neutron kinetic energy of the fragments is

$$\langle \mathrm{TKE}_{\mathrm{post}} \rangle = 199\ \mathrm{MeV}. \tag{20}$$

During the Geant4 simulation, whenever a ^{252}No recoil nucleus stopped in the active gas volume, one spontaneous-fission event was selected randomly from the pre-generated GEF library. Therefore, the fragment masses and fragment charges were not assigned independently but were taken directly from the same physical GEF event. The light and heavy fission fragments were then defined in Geant4 as ions with quantum numbers

$$(Z_L, A_{L,\mathrm{post}}) \qquad \text{and} \qquad (Z_H, A_{H,\mathrm{post}}), \tag{21}$$

respectively. This procedure preserves the event-by-event correlation between the two fragments and ensures consistency between the fragment species and the prompt-neutron multiplicity of the selected spontaneous-fission event.

The selected post-neutron fragment pair was emitted from the stopping point of the recoil nucleus. The fragment momenta were assigned in the rest frame of the fissioning nucleus under the condition of two-body momentum conservation,

$$\mathbf{p}_L + \mathbf{p}_H = 0, \qquad |\mathbf{p}_L| = |\mathbf{p}_H| = p. \tag{22}$$

The common momentum magnitude p was determined from the requirement that the sum of fragment kinetic energies reproduces the post-neutron TKE of the selected GEF event,

$$\mathrm{TKE}_{\mathrm{post}} = \left(\sqrt{p^2c^2 + m_L^2c^4} - m_Lc^2\right) + \left(\sqrt{p^2c^2 + m_H^2c^4} - m_Hc^2\right), \quad (23)$$

where m_L and m_H are the masses of the post-neutron light and heavy fragments, respectively. The individual fragment kinetic energies were then calculated as

$$E_L = \sqrt{p^2c^2 + m_L^2c^4} - m_Lc^2, \quad (24)$$

$$E_H = \sqrt{p^2c^2 + m_H^2c^4} - m_Hc^2, \quad (25)$$

so that

$$E_L + E_H = \mathrm{TKE}_{\mathrm{post}}. \quad (26)$$

As expected from two-body kinematics, the lighter fragment receives, on average, a larger fraction of the TKE.

The fission axis was generated isotropically in the rest frame of the stopped ^{252}No nucleus. The emission direction of the light fragment was sampled according to

$$\cos\theta \sim U(-1, 1), \qquad \varphi \sim U(0, 2\pi), \quad (27)$$

which defines the unit vector

$$\mathbf{n} = (\sin\theta\cos\varphi,\ \sin\theta\sin\varphi,\ \cos\theta). \quad (28)$$

The heavy fragment was emitted in the opposite direction,

$$\mathbf{n}_H = -\mathbf{n}_L. \quad (29)$$

Thus, both fragments originate from a common fission point and are initially emitted back-to-back.

Prompt neutrons were generated simultaneously with the two fission fragments. Their total multiplicity was taken directly from the GEF event,

$$\nu = \nu_L + \nu_H. \quad (30)$$

For each prompt neutron, the energy and angular coordinates from the `lmd+` event record were used. The neutron directions were given in the local fission-event coordinate system, defined relative to the light-fragment axis, and were subsequently rotated into the global Geant4 coordinate system. These neutrons were introduced as secondary tracks and transported through the detector materials using the activated Geant4 hadronic interaction models.

The initial kinetic energy of the primary ^{252}No recoil nucleus was sampled independently from the experimentally determined Gaussian distribution

$$E_{\mathrm{No}} \sim \mathcal{N}\left(17\ \mathrm{MeV}, (2.5\ \mathrm{MeV})^2\right). \quad (31)$$

The recoil ion was propagated through the detector geometry until it stopped. If the stopping point was located inside the active gas volume, a spontaneous-

fission event was generated at that position using the procedure described above. The two post-neutron fragments and all prompt neutrons were then transported through the full Geant4 detector geometry. Their trajectories and energy losses in the gas were used to determine the probability of registering both fission fragments in the sensitive TPC volume.

The calculated pre-neutron fragment-mass distributions were compared with the experimental data of Wild et al. [11]. The experimental mass yields for spontaneous fission of ^{252}No were taken from the EXFOR database, where the data are reported with a bin width of five mass units. To ensure a consistent comparison, the GEF distribution and the distribution reconstructed from the GEF events sampled in the Geant4 simulation were rebinned using the same bin width of five mass units. All three distributions were subsequently normalized over the full fragment-mass range. The resulting comparison is shown in Fig. 8.

As expected, the fragment-mass distribution reconstructed from the events sampled in Geant4 closely follows the original GEF distribution, confirming the correct transfer of the GEF fission-event information into the Geant4 simulation. The calculated distributions reproduce the general asymmetric two-peaked structure of the experimental pre-neutron mass distribution. At the same time, the calculated peaks are more pronounced and the distributions are narrower than those observed experimentally.

The TKE distribution of the fission fragments was validated in a similar way. The experimental TKE distribution for spontaneous fission of ^{252}No was taken from the EXFOR database, based on the measurements of

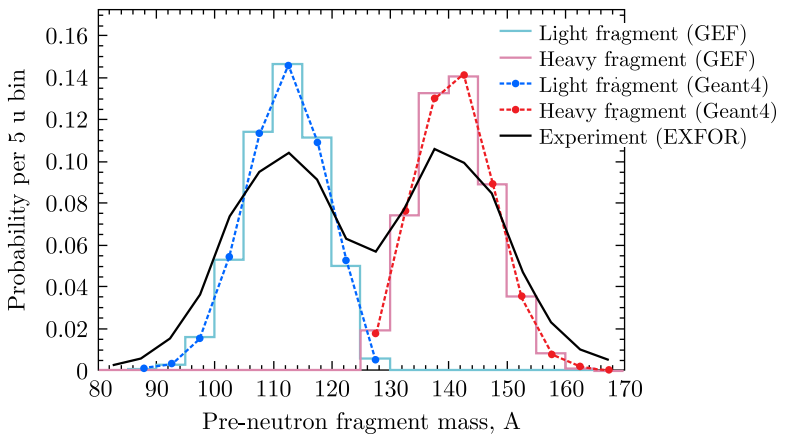


Fig. 8. Normalized pre-neutron fragment-mass distributions for spontaneous fission of ^{252}No obtained from GEF, from the GEF events sampled in the Geant4 simulation, and from the experimental EXFOR data. All distributions are presented using the same bin width of five mass units and are normalized over the full fragment-mass range

Wild et al. [11]. The experimental data are reported in intervals of 5 MeV. Therefore, both the GEF and Geant4 TKE distributions were rebinned using the same 5-MeV intervals and normalized over the considered energy range. The Geant4 distribution was obtained from 8259 fission events produced in a simulation of 10 000 primary ^{252}No nuclei. The resulting comparison is shown in Fig. 9.

The TKE distribution reconstructed from the Geant4 events closely follows the original GEF distribution over the entire considered energy range. This agreement provides an additional check that the fragment kinetic energies generated by GEF are transferred consistently to the Geant4 simulation. Both calculated distributions reproduce the overall shape and energy range of the experimental TKE distribution. However, the maximum of the experimental distribution is shifted towards somewhat lower TKE values compared with the GEF prediction, and differences in the detailed shape of the distributions remain visible.

Taken together, the comparisons of the fragment-mass and TKE distributions demonstrate that the implemented GEF–Geant4 interface consistently reproduces the fission-event information generated by GEF. The approach therefore provides a correlated event-by-event description of ^{252}No spontaneous fission in Geant4. In contrast to simplified models in which fragment masses, fragment charges, kinetic energies, and prompt-neutron multiplicities are sampled independently, the use of GEF `lmd+` events preserves their mutual correlations while allowing all generated particles to be transported through the detector using the standard Geant4 physics framework.

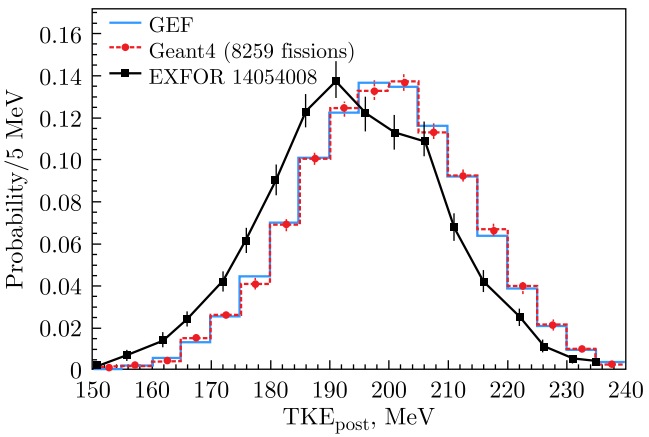


Fig. 9. Normalized TKE distributions for spontaneous fission of ^{252}No obtained from GEF, from the GEF events sampled in Geant4 simulation, and from the experimental EXFOR data. All distributions are presented using 5-MeV intervals

3.5. Influence of event statistics. The influence of the accumulated event statistics on the reconstructed fission observables was investigated using samples containing 10, 50, 100, and 200 ^{252}No fission events. The evolution of the post-neutron fragment-mass distribution with increasing statistics is shown in Fig. 10, while the corresponding TKE distributions are presented in Fig. 11.

At very low statistics ($N = 10$), both distributions are dominated by individual-event fluctuations and their characteristic shapes cannot be reliably identified. At $N = 50$, the underlying structures begin to emerge, although substantial bin-to-bin fluctuations remain. For approximately 100 fission events, the asymmetric two-peaked fragment-mass distribution becomes clearly distinguishable, and the TKE distribution begins to reproduce its characteristic broad structure. With 200 events, both distributions become considerably more stable.

These results indicate that approximately 100 fission events represent a reasonable minimum statistics for a qualitative identification of the main features of the fragment-mass and TKE distributions, while a sample of about 200 events provides a more robust representation of their shapes.

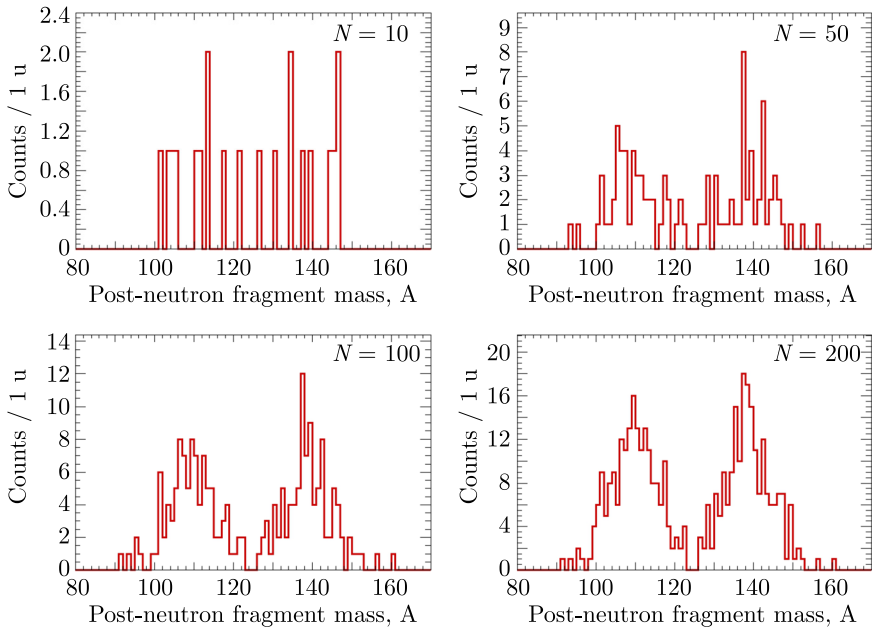


Fig. 10. Post-neutron fragment-mass distributions obtained from Geant4 simulations of ^{252}No spontaneous fission for samples containing 10, 50, 100, and 200 fission events. Both light and heavy fragments are included in each distribution. A bin width of one mass unit was used

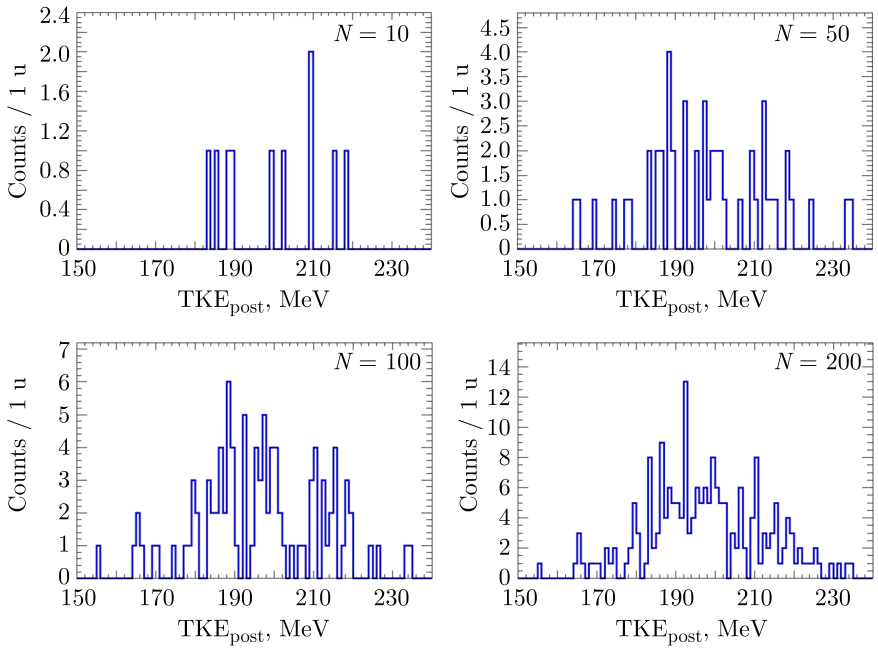


Fig. 11. Post-neutron TKE distributions obtained from Geant4 simulations of ^{252}No spontaneous fission for samples containing 10, 50, 100, and 200 fission events. A bin width of 1 MeV was used

3.6. Mechanical constraint on the Mylar separating foil. A thin Mylar foil is used as a separating element between the beam-line vacuum region and the gas volume of the TPC. Since the pressure in the separator region is of the order of 10^{-7}–10^{-6} mbar, it is negligible compared with the working gas pressure in the chamber. Therefore, the pressure difference acting on the foil can be approximated as

$$\Delta p \simeq p, \tag{32}$$

where p is the gas pressure in the detector volume.

The foil is supported by a cellular structure. As a result, the free span of the foil is not determined by the full entrance-window diameter, but by the size of a single support cell. In the present design, the support cell is approximated by an equivalent circular membrane with an effective radius

$$R = R_{\text{out}} - \Delta = 5.0 \text{ mm} - 0.5 \text{ mm} = 4.5 \text{ mm}, \tag{33}$$

where R_{out} is the distance from the cell center to the outer boundary of the hexagonal cell and Δ is the cell-wall thickness. The corresponding support-cell geometry is shown in Fig. 12.

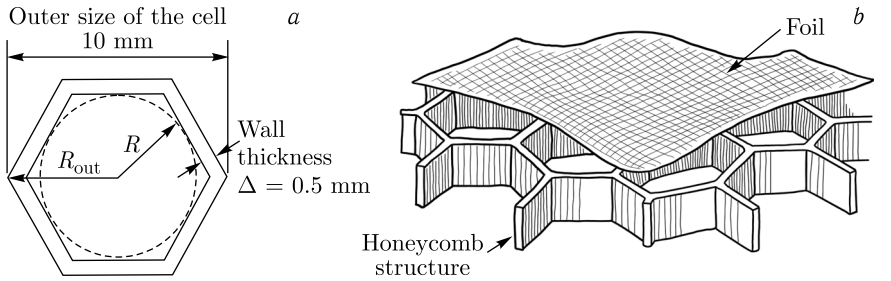


Fig. 12. Geometry of the Mylar foil support structure. *a*) Geometrical representation of a single hexagonal support cell used for the mechanical estimate of the foil, with an effective free-span radius $R = 4.5$ mm. *b*) Schematic illustration of the Mylar foil supported by the honeycomb structure

For a Mylar thickness in the micrometer range, the ratio between the characteristic free-span radius and the foil thickness is large. For example, for $t = 2$ μm one obtains

$$\frac{R}{t} \simeq \frac{4.5 \text{ mm}}{2 \ \mu\text{m}} \simeq 2 \cdot 10^3. \tag{34}$$

Thus, the foil thickness is several orders of magnitude smaller than the transverse dimension of the unsupported region. Under these conditions, the bending stiffness of the foil is negligible compared with membrane stretching, and the deformation can be described using the membrane approximation.

Although the real support geometry is hexagonal, it was replaced in the analytical estimate by an equivalent circular membrane with radius R. For a circular membrane with a clamped edge under uniform pressure, the maximum central deflection and membrane stresses can be estimated using the membrane approximation based on Hencky's solution [12–14]. They are written as

$$\delta_c = 0.662R \left(\frac{pR}{Et} \right)^{1/3}, \tag{35}$$

$$\sigma_c = 0.423 \left(\frac{Ep^2R^2}{t^2} \right)^{1/3}, \tag{36}$$

$$\sigma_{\text{edge}} = 0.328 \left(\frac{Ep^2R^2}{t^2} \right)^{1/3}, \tag{37}$$

where δ_c is the maximum central deflection, σ_c is the maximum central membrane stress, σ_{edge} is the stress near the edge, E is the Young modulus of the foil material, t is the foil thickness, and p is the pressure difference. Since the numerical coefficient in Eq. (36) is larger than that in Eq. (37), the maximum stress is expected in the central region of the membrane. Therefore, the rupture condition was defined by

$$\sigma_c = \sigma_{\text{lim}}, \tag{38}$$

where $\sigma_{\rm lim}$ is the tensile strength of Mylar. In the present estimate, typical room-temperature mechanical parameters of Mylar polyester film were used [15]. The tensile strength was taken as an engineering limiting value for the rupture estimate, while the Young modulus was used to characterize the elastic response of the membrane:

$$\sigma_{\rm lim} = 200 \text{ MPa}, \qquad E = 4.5 \text{ GPa}. \tag{39}$$

Substitution of Eq. (38) into Eq. (36) gives the burst pressure

$$p_{\rm break} = \frac{\sigma_{\rm lim}^{3/2} t}{0.423^{3/2} \sqrt{E}\, R}. \tag{40}$$

This expression shows that, for fixed material parameters and fixed support-cell size, the burst pressure is proportional to the foil thickness:

$$p_{\rm break} \propto t. \tag{41}$$

For the parameters used in the present geometry, this relation can be written in the convenient engineering form

$$p_{\rm break}(\text{atm}) \simeq 0.34\, t(\mu\text{m}). \tag{42}$$

In order to account for possible deviations from the ideal membrane model, material inhomogeneity, local stress concentration, and uncertainties in the boundary conditions, a safety margin was introduced. The safe working pressure was defined as

$$p_{\rm safe} = 0.7\, p_{\rm break}. \tag{43}$$

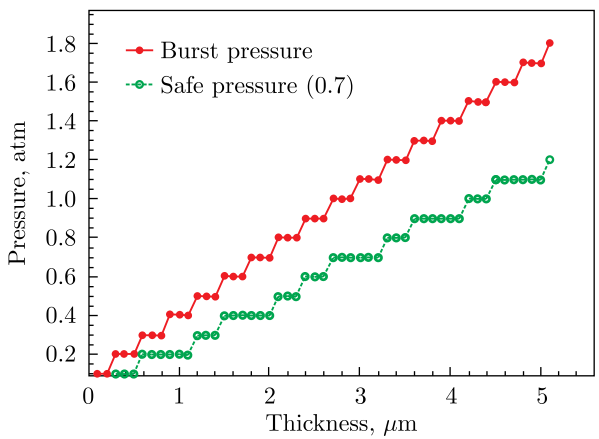


Fig. 13. Calculated burst pressure $p_{\rm break}$ and safe working pressure $p_{\rm safe} = 0.7 p_{\rm break}$ as functions of the Mylar foil thickness. The step-like behavior reflects the use of a finite set of technologically available foil thicknesses

This corresponds to a safety factor

$$\mathrm{FoS} = \frac{p_{\mathrm{break}}}{p_{\mathrm{safe}}} = \frac{1}{0.7} \simeq 1.4. \tag{44}$$

The calculated dependence of the burst pressure and the corresponding safe pressure on the Mylar thickness is shown in Fig. 13. Only working pressures below p_{safe} were considered mechanically acceptable in the subsequent optimization of the detector parameters.

3.7. Definition of the registration efficiency. The registration efficiency was used as the main quantitative criterion for evaluating the detector performance. In the present simulation, an event was considered successful if the recoil nucleus entered the detector through the entrance region, reached the predefined fission region, and the subsequent spontaneous-fission fragments were transported through the active gas volume in such a way that both fragment tracks could be registered by the TPC.

For each set of detector parameters, a fixed number of primary recoil nuclei was generated. The total number of generated events is denoted as N_{gen}. The number of events satisfying the registration criteria is denoted as N_{reg}. The registration efficiency was then defined as

$$\varepsilon = \frac{N_{\mathrm{reg}}}{N_{\mathrm{gen}}}. \tag{45}$$

The event-selection procedure included several consecutive conditions. First, the recoil nucleus had to pass through the geometrical entrance region of the detector. Events in which the recoil nucleus was lost in the entrance structures or did not reach the fission region were rejected. Second, the spontaneous-fission event had to occur in the predefined region of the detector geometry. Third, both fission fragments had to enter the active gas volume and produce tracks inside the sensitive region. Finally, the event was counted as registered only if the tracks of both fragments were sufficiently contained in the active volume to be suitable for event-by-event reconstruction.

Thus, the number of registered events can be written formally as

$$N_{\mathrm{reg}} = \sum_{i=1}^{N_{\mathrm{gen}}} \chi_i, \tag{46}$$

where χ_i is the registration indicator for the i-th simulated event:

$$\chi_i = \begin{cases} 1, & \text{if the event satisfies all registration criteria,} \\ 0, & \text{otherwise.} \end{cases} \tag{47}$$

In this definition, the efficiency characterizes the probability that a separator-delivered recoil nucleus produces a spontaneous-fission event whose two fragments can be reconstructed in the proposed TPC geometry. The criterion therefore includes both the transport of the recoil nucleus through

the entrance region and the registration of the two fission-fragment tracks in the active gas volume.

In addition to the geometrical and tracking criteria, the mechanical constraint imposed by the Mylar separating foil was taken into account. The detector configuration was considered mechanically acceptable only if the working gas pressure did not exceed the safe pressure defined in Eq. (43):

$$p \leqslant p_{\mathrm{safe}}(t), \tag{48}$$

where t is the Mylar foil thickness. Therefore, the optimization of detector parameters was performed only within the mechanically allowed region. Configurations with high registration efficiency but with a working pressure above the safe-pressure limit were excluded from the set of acceptable detector configurations.

The efficiency defined by Eq. (45) was calculated for different values of the working gas pressure and Mylar foil thickness. The resulting efficiency map was then used to determine the parameter region in which the proposed detector provides both efficient fission-fragment registration and mechanical stability of the separating foil.

4. RESULTS

The main result of the present optimization study is the registration-efficiency map of the proposed detector for the ^{252}No-based simulation. The efficiency was studied as a function of the Mylar entrance-window thickness and the working gas pressure. For each parameter combination, $N = 5000$ primary events were simulated, and the registration efficiency was calculated according to Eq. (45). The resulting two-dimensional distribution is shown in Fig. 14.

The efficiency map demonstrates that the detector response is determined by both the working gas pressure and the entrance-window thickness. At low pressures, the registration efficiency remains small because the stopping and detection conditions for recoil nuclei and fission fragments are unfavorable. At higher pressures, the efficiency increases; however, the operating pressure is limited by the mechanical stability of the Mylar foil.

The red curve in Fig. 14 corresponds to the calculated burst pressure of the foil, while the green dotted curve represents the safe working pressure defined by Eq. (43). Only configurations located on or below the safe-pressure curve were considered acceptable for practical operation. Therefore, the optimal detector parameters were selected from the mechanically safe part of the efficiency map.

For each point, the statistical uncertainty of the efficiency was estimated assuming binomial statistics,

$$\sigma_\varepsilon = 100\sqrt{\frac{\widehat{p}(1-\widehat{p})}{N}}, \qquad \widehat{p} = \frac{\varepsilon}{100}, \qquad N = 5000, \tag{49}$$

where ε is the registration efficiency in percent.

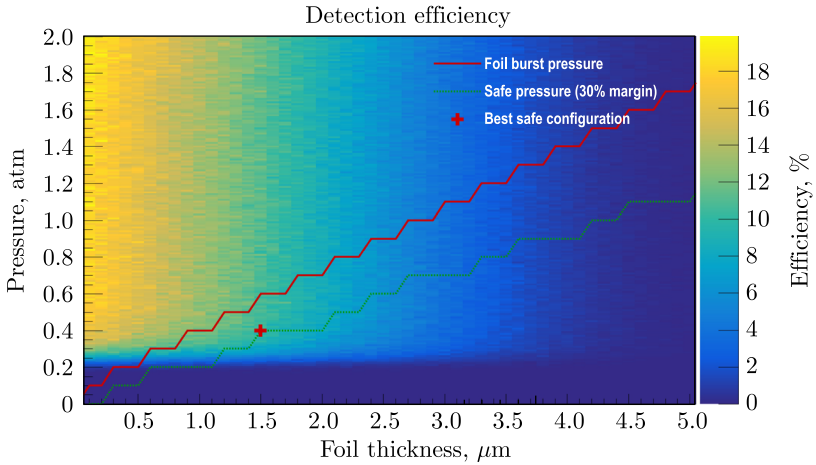


Fig. 14. Registration efficiency of the proposed TPC for ^{252}No as a function of the Mylar foil thickness and the working gas pressure. The red curve shows the burst-pressure limit of the separating foil, the green dotted curve corresponds to the safe working pressure with a 30% safety margin, and the red cross indicates the best mechanically safe detector configuration

The best mechanically safe configuration found in the present ^{252}No-based scan corresponds to a Mylar foil thickness of 1.5 μm and a working gas pressure of 0.40 atm. For this configuration, the calculated registration efficiency is

$$\varepsilon = (10.2 \pm 0.4)\%. \tag{50}$$

Here, the efficiency corresponds to the strict two-fragment registration criterion, in which an event is counted as successful only if both fission fragments are stopped and registered in the active gas volume.

The ten best mechanically safe configurations are listed in Table 2. The efficiencies of several neighboring configurations are close within the statistical uncertainty. Therefore, the result should be interpreted as a stable operating region rather than as a single sharply defined optimum.

The mechanically allowed region is defined by the condition

$$p \leqslant p_{\mathrm{safe}}(t), \tag{51}$$

where p is the working gas pressure and $p_{\mathrm{safe}}(t)$ is the safe pressure for a Mylar foil of thickness t. The highest-ranked configurations are concentrated mainly around foil thicknesses of 1.5–1.6 μm and pressures of 0.34–0.40 atm. This region provides a compromise between recoil transmission, stopping in the active gas volume, fission-fragment registration, and mechanical stability of the separating foil.

For the optimal configuration with a Mylar foil thickness of 1.5 μm and a gas pressure of 0.40 atm, an additional calculation with 10 000 primary events was performed. Out of these events, 8259 ^{252}No recoil nuclei reached the

Table 2. **Ten best mechanically safe detector configurations for the ^{252}No-based simulation. The uncertainty of the registration efficiency was calculated for $N = 5000$ simulated events for each configuration**

Rank	Foil thickness, μm	Pressure, atm	$\varepsilon \pm \sigma_\varepsilon$, %
1	1.5	0.40	10.2 ± 0.4
2	1.5	0.37	10.2 ± 0.4
3	1.5	0.34	10.0 ± 0.4
4	1.6	0.37	9.9 ± 0.4
5	1.2	0.30	9.9 ± 0.4
6	1.6	0.38	9.8 ± 0.4
7	1.6	0.39	9.7 ± 0.4
8	1.7	0.40	9.6 ± 0.4
9	1.6	0.40	9.5 ± 0.4
10	1.5	0.35	9.4 ± 0.4

active gas volume and stopped in it, corresponding to 82.6% of the primary events. The main loss of primary recoil nuclei was caused by the hexagonal supporting structure, where 17.38% of events were lost. The loss directly in the Mylar foil was only 0.03%.

In the 8259 simulated spontaneous-fission events, a total of 16 518 fission fragments were produced. Among these fragments, 55.52% stopped in the active gas volume, 16.10% were lost on the hexagonal supporting structure, 13.77% reached the stainless-steel chamber walls, 12.40% left the detector volume, and 2.20% were stopped in the Mylar foil.

With the strict two-fragment registration criterion, 1046 events out of 10 000 primary events were successfully registered. The corresponding absolute registration efficiency is

$$\varepsilon_{\mathrm{2frag}} = (10.5 \pm 0.3)\%. \tag{52}$$

The uncertainty was estimated assuming binomial statistics. This value is consistent with the result of the parameter scan, where the same detector configuration gave an efficiency of $(10.2 \pm 0.4)\%$ for 5000 primary events.

5. POSSIBLE OPERATION IN COMBINATION WITH SFiNx

The results discussed above were obtained using the strict registration criterion adopted for fission-fragment studies in the TPC. In that case, an event was counted as successfully registered only if both fission fragments were detected in the active gas volume. This criterion is appropriate for event-by-event reconstruction of fission-fragment observables, including TKE and fragment masses.

A different operating mode can be considered if the TPC is used together with the SFiNx neutron detector. In this case, the role of the TPC is not necessarily the full reconstruction of both fragments, but rather the identification of the spontaneous-fission event and the determination of its time. Once such a charged-particle signal is registered in the active gas

volume, it can be used as a trigger for the search for prompt neutrons in the surrounding SFiNx detector.

The SFiNx detector is based on ^{3}He proportional counters placed in a moderator. Prompt neutrons emitted in spontaneous fission are slowed down in the moderator and then detected through the capture reaction

$$n + {}^3\mathrm{He} \to p + {}^3\mathrm{H} + 764\ \mathrm{keV}. \tag{53}$$

According to the current SFiNx characteristics, the single-neutron registration efficiency is about $(55 \pm 1)\%$, while the average neutron lifetime in the assembly is about $(18 \pm 1)\ \mu$s [1].

The compact TPC geometry considered in the present work is compatible with the central region of the SFiNx detector. In such a configuration, the TPC replaces the original central gas chamber, while the surrounding neutron-counter geometry is preserved. The SFiNx detector and the corresponding TPC placement scheme are shown in Fig. 15.

For this combined TPC–SFiNx operating mode, the event-selection criterion can be relaxed. Instead of requiring the registration of both fission fragments in the active gas volume, an event can be counted as useful if at least one of the two fission fragments is stopped and registered in the gas. Such a signal is sufficient to confirm the occurrence of spontaneous fission and to define the reference time for the prompt-neutron search.

For the optimized geometry, this relaxed criterion gives 8125 successful events out of 10 000 simulated spontaneous-fission events. The corresponding absolute efficiency is

$$\varepsilon_{\geqslant 1} = (81.3 \pm 0.4)\%. \tag{54}$$

The uncertainty was estimated assuming binomial statistics.

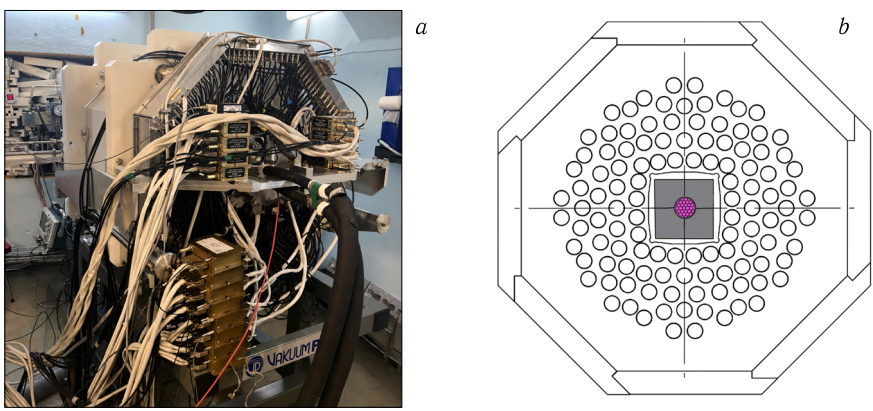


Fig. 15. Possible combined TPC–SFiNx configuration. *a*) Photograph of the SFiNx detection system installed at the focal plane of the SHELS velocity filter. *b*) Schematic placement of the proposed compact TPC in the central region of the SFiNx neutron-detector assembly, with the surrounding ^{3}He neutron-counter geometry preserved

This value is much higher than the efficiency obtained with the strict two-fragment criterion. Therefore, while the strict criterion is required for detailed reconstruction of fission-fragment observables, the relaxed one-fragment criterion is more suitable for a combined TPC–SFiNx experiment aimed at prompt-neutron studies. In this mode, the TPC provides a charged-particle confirmation of the spontaneous-fission event and a time reference for neutron-correlation analysis, while SFiNx provides prompt-neutron multiplicity information.

CONCLUSIONS

A concept of a GRAND-coupled time-projection chamber for studies of spontaneous fission of heavy and superheavy nuclei has been proposed. The detector is intended for operation at the GRAND focal plane. In the proposed configuration, evaporation residues separated by GRAND pass through an entrance window and stop in the active gas volume of the chamber, where subsequent spontaneous-fission fragments can be registered.

A Geant4-based simulation model was developed for conditions corresponding to ^{252}No recoil nuclei produced in the ^{206}Pb(^{48}Ca, $2n$)^{252}No reaction. The model included the transverse recoil-nucleus distribution at the detector entrance, the experimentally based recoil-energy distribution, the transport and stopping of recoil nuclei, and the generation and transport of spontaneous-fission fragments in the active gas volume.

The influence of the Mylar entrance-window thickness and the working gas pressure on the registration efficiency was investigated. The mechanical stability of the separating foil was included as an additional constraint through the safe-pressure condition. The best mechanically safe configuration found in the present ^{252}No-based parameter scan corresponds to a Mylar foil thickness of 1.5 μm and a working gas pressure of 0.40 atm. For this configuration, the calculated efficiency for the strict two-fragment registration criterion is $(10.2 \pm 0.4)\%$. An additional calculation with 10 000 primary events gave a consistent value of $(10.5 \pm 0.3)\%$.

For this optimized configuration, 82.6% of the primary ^{252}No recoil nuclei reached the active gas volume and stopped in it. The main loss of primary recoil nuclei was caused by the hexagonal supporting structure, while the loss directly in the Mylar foil was negligible. The analysis of fission-fragment transport showed that the registration efficiency is limited not only by the stopping of the recoil nuclei but also by the subsequent propagation of the two fission fragments in the compact detector geometry.

The proposed TPC can extend spontaneous-fission measurements from event identification to event-by-event information on fission-fragment kinematics. After appropriate calibration, track and energy-loss information in the active gas volume may provide constraints on the reconstruction of TKE and fragment masses. The detector may also be useful for identifying rare fission modes, such as ternary-fission candidates.

A separate operating mode was considered for possible combined measurements with the SFiNx neutron detector. In this case, the full reconstruction of both fission fragments is not required: registration of at least one fission fragment in the active gas volume is sufficient to confirm the spontaneous-fission event and to define the reference time for the prompt-neutron search. For the optimized geometry, this relaxed one-fragment criterion gives an absolute efficiency of $(81.3 \pm 0.4)\%$. This value indicates that the proposed compact TPC geometry can be suitable not only for detailed fission-fragment studies but also for TPC–SFiNx experiments aimed at prompt-neutron multiplicity measurements.

The present work should be regarded as a simulation and design study. Further development should include a more detailed detector-response model, including electron drift, diffusion, gas amplification, charge collection, electronic thresholds, and signal reconstruction. Prototype tests with calibration sources and heavy-ion beams will be required to validate the entrance-window design and the reconstruction of fission-fragment observables.

Acknowledgements. The initial development of the present work was carried out as part of I. I. Ulanova's diploma thesis under the scientific supervision of A. V. Isaev.

Author contributions. I. I. Ulanova: conceptualization, methodology, software, data curation, formal analysis, investigationl, visualization, writing — original draft; A. V. Isaev: supervision, validation, conceptualization, methodology; R. S. Mukhin: validation, conceptualization, methodology; A. M. Solntsev: software, methodology; V. I. Chepigin, O. N. Malyshev, I. N. Izosimov, and E. A. Sokol: methodology, validation; Yu. A. Popov: resources, methodology; G. Kaminski, A. V. Karpov, and A. I. Svirikhin: validation, project administration.

All authors discussed the detector design, contributed to the scientific content of the manuscript, participated in writing — review and editing, and approved the final version.

Funding. This work was supported by ongoing institutional funding. No additional grants to carry out or direct this particular research were obtained.

Conflicts of interest. The authors declare no conflicts of interest.

Data availability statement. The simulation input parameters, processed numerical data, and data used to produce the figures and tables in this study are available from the corresponding author upon reasonable request.

REFERENCES

1. *Isaev A. V., Mukhin R. S., Andreev A. V., Chelnokov M. L., Chepigin V. I., Devaraja H. M., Izosimov I. N., Katrasev D. E., Kuznetsova A. A., Malyshev O. N., Popeko A. G., Popov Yu. A., Rahmatinejad A., Sailaubekov B., Shneidman T. M.,*

Sokol E. A., Svirikhin A. I., Tezekbayeva M. S., Yeremin A. V. The SFiNx Detector System (Current Status) // Phys. Part. Nucl. Lett. 2025. V. 22. P. 300–303; DOI: 10.1134/S1547477124702303.

2. *Isaev A. V., Yeremin A. V., Zamyatin N. I., Izosimov I. N., Kuznetsova A. A., Malyshev O. N., Mukhin R. S., Popeko A. G., Popov Yu. A., Sailaubekov B., Svirikhin A. I., Sokol E. A., Tezekbayeva M. S., Testov D. A., Chelnokov M. L., Chepigin V. I., Antalic S., Mosat P., Brionnet P., Gall B.* The SFiNx Detector System // Phys. Part. Nucl. Lett. 2022. V. 19. P. 37–45; DOI: 10.1134/S154747712201006X.
3. *Popeko A. G.* On-Line Separators for the Dubna Super Heavy Element Factory // Nucl. Instr. Meth. Phys. Res. B. 2016. V. 376. P. 144–149; DOI: 10.1016/j.nimb.2016.02.025.
4. *Kuznetsova A. A.* First Tests of the GRAND Gas-Filled Separator at the Superheavy Element Factory (Flerov Laboratory of Nuclear Reactions, Joint Institute for Nuclear Research) // Bull. Russ. Acad. Sci. Phys. 2023. V. 87. P. 1105–1111; DOI: 10.3103/S1062873823702921.
5. *NIFFTE Collab.: Heffner M., Asner D. M., Baker R. G., Baker J., Barrett S., Brune C., Bundgaard J., Burgett E., Carter D., Cunningham M., Deaven J., Duke D. L., Greife U., Grimes S., Hager U., Hertel N., Hill T., Isenhower D., Jewell K., King J., Klay J. L., Kleinrath V., Kornilov N., Kudo R., Laptev A. B., Leonard M., Loveland W., Massey T. N., McGrath C., Meharchand R., Montoya L., Pickle N., Qu H., Riot V., Ruz J., Sangiorgio S., Seilhan B., Sharma S., Snyder L., Stave S., Tatishvili G., Thornton R. T., Tovesson F., Towell D., Towell R. S., Watson S., Wendt B., Wood L., Yao L.* A Time Projection Chamber for High Accuracy and Precision Fission Cross-Section Measurements // Nucl. Instr. Meth. Phys. Res. A. 2014. V. 759. P. 50–64; DOI: 10.1016/j.nima.2014.05.057.
6. *Kubiela A., Ahn D.-S., Baba H., Bezbakh A., Ciemny A. A., Dominik W., Fukuda N., Giska A., Grzywacz R., Guadilla V., Ichikawa Y., Janas Z., Janiak L., Kaminski G., Kawata K., Kubo T., Madurga M., Mazzocchi C., Nishibata H., Pomorski M., Shimizu Y., Sokolowska N., Suzuki D., Suzuki H., Szymkiewicz P., Swiercz A., Tajima M., Takamine A., Takeda H., Takeuchi Y., Thornsberry C. R., Ueno H., Yamazaki H., Yokoyama R., Yoshida K., Pfutzner M.* Decay Study of the Most Neutron-Deficient Zn Isotopes with the Warsaw Optical TPC Detector. arXiv:2509.25061 [nucl-ex]. 2025; DOI: 10.48550/arXiv.2509.25061.
7. *Geant4 Collab.* Geant4 — A Simulation Toolkit // Nucl. Instr. Meth. Phys. Res. A. 2003. V. 506. P. 250–303; DOI: 10.1016/S0168-9002(03)01368-8.
8. *Geant4 Collab.* Recent Developments in Geant4 // Nucl. Instr. Meth. Phys. Res. A. 2016. V. 835. P. 186–225; DOI: 10.1016/j.nima.2016.06.125.
9. *Giomataris Y., Rebourgeard Ph., Robert J. P., Charpak G.* MICROMEGAS: A High-Granularity Position-Sensitive Gaseous Detector for High Particle-Flux Environments // Nucl. Instr. Meth. Phys. Res. A. 1996. V. 376. P. 29–35; DOI: 10.1016/0168-9002(96)00175-1.
10. *Schmidt K.-H., Jurado B., Amouroux C., Schmitt C.* General Description of Fission Observables: GEF Model Code // Nucl. Data Sheets. 2016. V. 131. P. 107–221; DOI: 10.1016/j.nds.2015.12.009.
11. *Wild J. F., Hulet E. K., Lougheed R. W., Moody K. J., Bandong B. B., Dougan R. J., Veeck A.* Spontaneous Fission Properties of ^{252,254}No and ^{256,258} [104] and the

Disappearance of the Outer Fission Barrier // J. Alloys Compd. 1994. V. 213–214. P. 86; DOI: 10.1016/0925-8388(94)90885-0.
12. *Hencky H.* Über den Spannungszustand in kreisrunden Platten mit verschwindender Biegungssteifigkeit // Z. Math. Phys. 1915. V. 63. P. 311–317.
13. *Huang S. C.* Hencky's Solution for Circular Membranes under Pressure. NASA Technical Report, 1997.
14. U.S. Air Force, Air Force Stress Manual, Section on membranes, 1986.
15. DuPont Teijin Films. Mylar® Polyester Film: Physical-Thermal Properties. Product Information. 2003.

Received on September 1, 2026.

Редактор *Е. И. Крупко*

Подписано в печать 16.10.2026.
Формат 60 × 90/16. Бумага офсетная. Печать цифровая.
Усл. печ. л. 2,00. Уч.-изд. л. 2,45. Тираж 85 экз. Заказ № 61376.

Издательский отдел Объединенного института ядерных исследований
141980, г. Дубна, Московская обл., ул. Жолио-Кюри, 6.
E-mail: publish@jinr.ru
publish.jinr.ru